Check for updates

A new graphene-based nanomaterial increases lipolysis and reduces body weight gain through integrin linked kinase (ILK)†

Sergio de Frutos, [iD] *[a,b] Mercedes Griera,[c] Maria del Prado Lavín-López, [iD] [d] Martín Martínez-Rovira,[d] José António Martínez-Rovira,[d] Manuel Rodríguez-Puyol[a,b] and Diego Rodríguez-Puyol[e,b]

White adipose tissue (WAT) hypertrophy is caused by the excessive storage of triglycerides (TGs) and is associated with obesity. We previously demonstrated that extracellular matrix mediator integrin beta1 (INTB1) and its downstream effector integrin linked kinase (ILK) are implicated in obesity establishment. We also considered in our previous works that ILK upregulation is a therapeutical strategy to reduce WAT hypertrophy. Carbon based nanomaterials (CNMs) have interesting potential to modify cell differentiation but have been never studied to change the properties of adipocytes. Methods: GMC is a new graphene-based CNM that was tested for biocompatibility and functionality in cultured adipocytes. MTT, TG content, lipolysis quantification, and transcriptional changes were determined. Specific INTB1 blocking antibody and ILK depletion with specific siRNA were used to study the intracellular signalling. We complemented the study using subcutaneous WAT (scWAT) explants from transgenic ILK knockdown mice (cKD-ILK). GMC was topically administrated in the dorsal area of high fat diet-induced obese rats (HFD) for 5 consecutive days. The scWAT weights and some intracellular markers were analyzed after the treatment. Results: graphene presence was characterized in GMC. It was non-toxic and effective in reducing TG content *in vitro* in a dose-dependent manner. GMC rapidly phosphorylated INTB1 and increased the expression and activity of hormone sensitive lipase (HSL), the lipolysis subproduct glycerol, and the expression of glycerol and fatty acid transporters. GMC also reduced the expression of adipogenesis markers. Pro-inflammatory cytokines were unaffected. ILK was overexpressed, and INTB1 or ILK blockade avoided functional GMC effects. Topical administration of GMC in HFD rats overexpressed ILK in scWAT, and their weight gains were reduced, while systemic (renal, hepatic) toxicity parameters were unaffected. Conclusions: GMC is safe and effective in reducing hypertrophied scWAT weight when topically applied and it can be considered of interest in anti-obesogenic strategies. GMC increases lipolysis and reduces adipogenesis inside adipocytes by mechanisms that imply the activation of INTB1, the overexpression of ILK, and changes in the expression and activity of several markers related to fat metabolism.

[a]*Department of Systems Biology of Universidad de Alcalá (UAH), 28805 Alcalá de Henares, Madrid, Spain. E-mail: sergio.frutos@uah.es; Tel: +34918854519*
[b]*Instituto Ramon y Cajal de Investigación Sanitaria (IRYCIS), Fundación Renal Iñigo Álvarez de Toledo (FRIAT), RICOR from Instituto de Salud Carlos III and NOVELREN from Comunidad de Madrid, Spain*
[c]*Graphenano Medical Care S.L., Madrid, Spain*
[d]*Graphenano S.L., Murcia, Spain*
[e]*Department of Medicine of Universidad de Alcalá (UAH), Nephrology Department at Hospital Príncipe de Asturias, Instituto Ramon y Cajal de Investigación Sanitaria (IRYCIS), Fundación Renal Iñigo Álvarez de Toledo (FRIAT), RICOR from Instituto de Salud Carlos III and NOVELREN from Comunidad de Madrid, Spain*
†Electronic supplementary information (ESI) available. See DOI: https://doi.org/10.1039/d2bm01791a

1. Introduction

Several metabolic disorders are referred and interlinked to TG metabolism and adipocyte size misfunction, such as obesity, diabetes mellitus type 2, non-alcoholic fatty liver disease, atherosclerosis, and arterial damage. Adipocytes are the main cell population present within the white adipose tissue (WAT), which preserves energy homeostasis and body weight, and it is distributed in different located depots, from subcutaneous areas (scWAT) to the abdominal cavity.[1] WAT enlargement is associated by either the proliferation of new adipocytes (hyperplasia) or the increase of intracellular TG storage (hypertrophy). Stem pre-adipocytes as well as new and resident adipo-

cytes may trans-differentiate and change intracellular volumes adapting to the storage of triglycerides (TG) in the lipid droplet (LD). The TG metabolic cycle is comprised of its intracellular formation (lipogenesis) and catabolism (lipolysis), plus the metabolite (fatty acids and glycerol) efflux through the adipocyte membranes. Enlargement of scWAT occurs mostly because of the hypertrophic differentiation of the existing adipocytes.[2,3] Therefore, therapeutic strategies are looking for compounds that artificially hinder or obstruct the hypertrophic differentiation of distressed adipocytes. The mechanisms followed by the extracellular moiety that surrounds the adipocytes inside WAT, either soluble substances as growth factors or structural components featured in the extracellular matrix (ECM), can be considered in the thinking and design of those future therapeutical fat modulators.[4] To our knowledge, this has not been considered for carbon nanomaterials (CNMs), which are promising bioactive nanostructures that may mimic ECM-cell interactivity, promoting cell adhesion, spreading, growth, and differentiation routes.[5,6] CNMs are classified according to their structural diversity.[7] Graphene-based CNM, such as graphene oxide (GO), reduced graphene oxide (rGO), carbon nanotubes (CNTs) or carbon nanofibers (CNFs), share different arrangements of graphene in their structure, which is defined as one carbon atom thick disposition that features exceptionally large and reactive surface area. CNF has been applied in biomedical fields for more than 30 years and got intrinsic advantages compared to the extensively investigated GO or CNT, such as more electric conductivity, larger scale manufacturing, and biocompatibility during production.[8–10] Each CNM may interact with the cell by different operating mechanisms because of the ultrastructure physicochemical particularities.[11] It has been hypothesized that graphene bioactivity may start with the interaction of transmembrane receptors integrins (INT), which orchestrate the ECM-based (outside-in) signaling that regulates the intracellular architecture and transcription of genes.[12–16]

In WAT, integrin β1 subunit (INTB1) is a determinant for several adipocyte events such as differentiation to adipogenesis, insulin signaling, LD storage, and TG metabolites trafficking[17] and requires phosphorylation to be conformationally active to recruit intracellular downstream cytoskeleton and other scaffold proteins.[18] We and others recently discovered that the presence of the INTB1 scaffold protein Integrin Linked Kinase (ILK)[19] is of interest during WAT remodeling[20–23] and we defined that ILK pharmacological upregulation in WAT ameliorates adipogenesis and hypertrophy in a pro-obesogenic model *in vivo*. Importantly, some publications have pointed to some CNM to modify ILK expression and activity during stem cell differentiation.[14,16] Taking all this into consideration, we hypothesized that CNF structure may interact with INTB1-ILK to change adipocyte pattern, and here, we feature evidence and provide some mechanistic insights for the anti-obesogenic/fat-reducing use of a new biocompatible and size-delimited CNF-based material named GMC.

2. Materials and methods

2.1. GMC preparation and characterization

GMC was obtained from the purification and bio compatibilization of CNF with high surface supplied by Graphenano S.L. CNF was treated overnight in a strong acid solution to remove impurities and washed with distilled water until reaching neutral pH. GMC was subjected to a standard depyrogenization process at temperatures around 400 °C under inert atmosphere (with high purity grade nitrogen). GMC particle size was reduced and controlled through an exfoliation process and filtration system. Characterization techniques for raw CNF material and GMC were achieved as previously described.[24] Raman spectroscopy was performed using a Senterra spectrometer with a grating of 600 lines per mm and a laser wavelength of 532 nm at <1 mW laser power level (Bruker Española, Madrid, Spain). Crystallographic X-ray diffraction parameters were determined using a diffractometer Phillips PW-1711 with a uKa radiation and 1.5404 Å wavelength. Interlaminar distance was calculated with Braggs's equation $\lambda/2 \cdot \sin(\theta)$, where λ is 1.5404 Å long wave radiation and θ is the diffraction angles of [002] and [001] peaks (which correspond to the stacking aromatic structure and the orientation of graphene layer planes, respectively). Crystalline size in the perpendicular plane, or crystal stack height of graphene layers, is obtained with Scherrer's equation $L_c = K_c \cdot \lambda / \text{FWHM} \cdot \cos(\theta)$, where K_c is the carbonous constant (= 0.9) and FWHM, Full Width at Half Maximum of the corresponding diffraction peak (in rad units). Particle size distribution was determined by dynamic light scattering with ZetaSizer Nano Series (Malvern Panalytical Ltd, Malvern, UK). Scanning electron microscopy images were obtained using Zeiss GeminiSE500 equipment with a thermal field emission, an acceleration voltage from 0.02–30 kV, and a magnification from 50 to 2 000 000. High resolution transmission electron microscopy was performed using an FEI Tecnai G2 F20 S-TWIN equipment. As negative controls in comparative functional studies, other carbon materials were used in the same concentrations and conditions as GMC, such as carbon black, GO and rGO (all from Merck-Millipore, Billerica, MA, USA).

2.2. Culture and differentiation of adipocytes

C3H10T1/2 preadipocytes (CCL-226, ATCC, Manassas, USA) were grown on 6-well plates with DMEM (Sigma-Aldrich, St Louis, MO, USA) and 10% fetal bovine serum (FBS, Thermo Fisher Scientific Waltham, MA, USA). 2 days after confluency, cells were treated with differentiation medium for 48 h: DMEM supplemented with 10% FBS, Glutamax (Thermo Fisher Scientific), 1 μM dexamethasone, 1 μM rosiglitazone, 0.5 mM 3-isobutyl-1-methylxanthine (IBMX), and 5 μg mL⁻¹ insulin (Sigma-Aldrich). Medium was replaced every two days for a total of 6–10 days with DMEM supplemented with 10% FBS Glutamax and 5 μg mL⁻¹ insulin. The 9th day from the beginning of the differentiation, adipocytes were deprived of any supplementation for 24 h, prior to any treatment.[23] Treatments, including GMC or vehicle (VH) as control (CT),

were added for the indicated times under deprived conditions to avoid any biological effect from soluble factors present in the growing medium. Safety of GMC was tested after treatment by measuring nuclear trypan blue dye exclusion and the determination of mitochondrial metabolic activity (MTT).

2.3. Adipocytes transient transfection with siRNAs

Fully differentiated adipocytes were plated at 70–80% confluence in 6 well plates. After 24 h, adhered adipocytes were transfected with 20 nM specific silencing RNAs (siRNA) against ILK (siILK, Santa Cruz Biotechnologies Inc., Dallas, TX) or scramble siRNAs with Metafectene (Biontex, Munich, Germany) overnight and allowed to recover for 48 h, the first 24 h with DMEM with serum for another 24 h and deprived for another 24 h.[23] Deprivation of serum assures that the GMC and VH experimental groups started in the same post-transfection conditions. Treatments were performed thereof for the indicated times. Successful ILK depletion was checked after all the procedures by determining ILK mRNA levels.

2.4. Animal models

Animal experiments have been approved by the Institutional Animal Care and Use Committees from Universidad de Alcalá and Comunidad de Madrid (PROEX 230/16), in agreement with the guidelines established by the European Community Council Directives (2010/63/EU). Age-matched male and female adult conditional ILK-deficient mice (cKDILK) and wild-type counterparts (WT) were generated, divided randomly and subjected to High Fat diet (HFD, 60 kJ% fat, 8.46% sucrose; D12492 Ssniff Spezialdiäten, Soest, Germany) to allow the establishment of obesity and the increase of WAT depots sizes, or the corresponding low fat standard diet (STD, 13 kJ% fat, 67 kJ% carbohydrates, 10% sucrose; Envigo Teklad Global Diet 2014, East Millstone, NJ, USA), as detailed in our previous works.[21–23] Briefly, general inactivation of the ILK gene in our implemented cKD-ILK model was accomplished by crossing C57Bl/6 mice homozygous for the floxed Ilk allele, flanked by loxP sites (LOX) with homozygous BALB/cJ strain mice carrying a CMV-driven tamoxifen-inducible CreER (T) recombinase gene (CRE); three-month-old male CRE-LOX weighing 20 to 28 g were injected intraperitoneally (i.p.) with 1.5 mg of 4-hydroxytamoxifen (TX, Sigma-Aldrich, St Louis, MO, USA) or vehicle (VH, corn oil/ethanol, 9:1, Sigma-Aldrich, St Louis, MO, USA) once a day for five consecutive days. Three weeks after the injections, the tail DNA was genotyped by PCR. The TX-treated CRE-LOX mice displaying successful depletion of ILK were termed cKD-ILK and the VH-treated CRE-LOX were termed wild-type (WT) mice. After the diet challenges, scWAT explants from the dorsal-inguinal area were extracted and incubated ex vivo with treatments in the same conditions as in vitro cultured cell experiments. In vivo applications of formulated products were performed in Wistar rats (Janvier Labs, Genest-Saint-Isle, France). Briefly, age-matched male and female rats were divided randomly and fed for 5 weeks with either STD or HFD as described elsewhere.[25] At the beginning of the 6th week, animals were weighed, and dorsal-inguinal areas were depilated. Each experimental diet group was randomly divided in two, where each sub-group was subjected to the topical applications in the depilated dorsal-inguinal area of formulated forms based on pure paraffin with either GMC or VH as described.[26] The application was performed with massage 2 times per day for a total period of 5 days while the animals were maintained in their diets. At the end of the experiments, animals were euthanized, weighed and blood samples extracted. Each animal had free access to water and was kept on a 12:12 h light:dark cycle at a constant temperature of 21–23 °C. Diets and water were supplied ad libitum. The food and water intakes were calculated by subtracting the mass of food or volume of water left from the initial supply. Fasting glucose was determined using a glucometer via tail bleeding (Accu-Check Aviva; Roche, Basel, Switzerland).[22]

After the experimentation concluded, animals were maintained under fasting conditions for 16 h, weighed, and euthanized with pentobarbital overdose. Body weight gains were calculated by subtracting weights at the beginning from weights at the end of each experimental timeline. Dorsal-inguinal scWAT depots were dissected, weighed, and divided to perform ex vivo experiments or preserved in RNAlater (Thermo Fisher Scientific, Waltham, MA, USA) for future determinations. Blood was extracted from animals and creatinine and aspartate aminotransferase in plasmas were determined using commercial kits. Peripheral blood mononuclear cells (PBMC) were purified and Interleukin-1β mRNA was determined by RT-qPCR.

2.5. Intracellular triglyceride quantification

Fully differentiated adipocytes were deprived, treated, washed, and stained after the indicated times with the lipid dye AdipoRed (Lonza, Basel, Switzerland) as indicated by the commercial manual. Fluorimetry was quantified with 485 nm excitation/572 nm emission using a VictorX4 plate reader (PerkinElmer) and values were normalized to total protein content per well, determined by DC-Protein Assay (Bio-Rad, Hercules, CA, USA). A filtered dilution of Oil Red O (Sigma-Aldrich, 0.3 g in 100 mL of 60% isopropanol) was used on cells fixed with 4% formaldehyde, and pictures were taken using an inverted microscope.[23]

2.6. Reverse transcription–quantitative polymerase chain reaction (RT-qPCR)

All products and equipment used were from Thermo Fisher Scientific. After the corresponding experiment, total RNA was extracted from cells or tissues collected from fasting mice. Equal amounts of RNA were transcribed to cDNA with HighCapacity cDNA RT Kit, and 10 ng of cDNAs were amplified using kits for qPCR. TaqMan gene expression assays were used to quantify monocyte chemoattractant protein-1 (MCP-1, Mm00441242_m1), Interleukin-6 (IL-6, Mm00446190_m1), peroxisome proliferator activated receptor gamma (PPARγ, Mm00440940_m1), Leptin (Mm00434759_m1), CCAAT/enhancer-binding protein beta (CEBP, Mm00514283_s1), fatty acid binding protein 4 (FABP4, Mm00445878_m1), aquaporin 7 (AQP7, Mm00431839-m1), fatty acid translocase (FAT,

Mm00432403_m1), hormone-sensitive lipase (HSL, Mm00495359_m1), Interleukin-1β (IL-1β, Mm00434228_m1), Peroxisome Proliferator-activated Receptor Gamma-coactivator-Alpha (PGC1-alpha, Mm01208835_m1), Fatty acid synthase (FASN, Mm00662319_m1), and β-actin (Mm01205647_g1). Amplification values were normalized to endogenous β-actin and relative quantification was determined with the $2^{-\Delta\Delta CT}$ method. To quantify the non-excised ILK sequence between exons within the floxed area number 6 and 7 in WT and cKD-ILK specially designed primers (GGGCTCTTGTGAGCTTCTGT and GAGTGGTCCCCTTCCAGAAT) and glucose transporter type4 (GLUT4, ATGGCTGTCGCTGG-TTTCTC and TAAGGACCCATAGCATCC) were determined with SYBR Green Master Mix and normalized to β-actin (GACGGCCAGGTCATCACTAT and CTTCTGCATCCTGTCAGCAA).[22,23]

2.7. Protein extraction and immunoblot analysis

Cells were homogenized in lysis buffer (10 mM Tris-HCl, pH 7.6; 1% Triton X-100; 1 mM EDTA; 0.1% sodium deoxycholate) supplemented with protease and phosphatase inhibitors (Complete and PhosSTOP, Roche, Basel, Switzerland). Protein concentrations were determined by DC-Protein Assay (Bio-Rad, Hercules, CA, USA). Equal amounts were separated on SDS-polyacrylamide gels and transferred to 0.2 μm PVDF membranes (Bio-Rad, Hercules, CA, USA). Membranes were blocked and incubated with primary antibodies and secondary antibodies (Merck-Millipore, Billerica, MA, USA or Dako, Glostrup, Denmark) afterwards. Primary antibodies were used against ILK (4G9), HSL, its active isoform, phosphorylated at ser660 ser 660 (P-HSL) (Cell Signaling Technology, Danvers, MA, USA), INTB1, its active isoform, phosphorylated at thr 788/9 (P-INTB1, Abcam, Cambridge, United Kingdom), Tubulin, Actin or GAPDH (Sigma-Aldrich, St Louis, MO, USA). Immunoblots were detected by chemiluminescence (Pierce ECL Western Blotting Substrate, Thermo Fisher Scientific Waltham, MA, USA) and imaged with ImageQuant LAS 500 System (General Electric Healthcare, Little Chalfont, United Kingdom). Densitometries were measured using ImageJ software (NIH).

2.8. Free glycerol measurement in supernatants and glucose uptake assay

Fully differentiated adipocytes deprived of serum or dorsal-inguinal scWAT depots weighed and divided were treated in DMEM free of serum for the indicated times. Excreted glycerol was measured in the supernatants using a commercial ELISA-based assay kit (BioVision, Milpitas, CA, USA) according to the manufacturer's instructions and normalized to total protein content. Glucose uptake was performed as described previously.[21] Briefly, samples were incubated in DMEM free of serum, glucose, and sodium pyruvate (Thermo Fisher Scientific Waltham, MA, USA). Insulin (100 nM, Actrapid, Novo Nordisk A/S, Bagsværd, Denmark) was added for additional 15 min and 0.1 mM of the fluorescent D-glucose analogue 2-[N(7nitrobenz-2-oxa-1,3-diazol-4-yl)amino]-2-deoxy-glucose (2-NBDG, Sigma-Aldrich, St Louis, MO, USA) was added for 30 min more. Free 2-NBDG was washed out 3 times with cold PBS, tissues were lysed and intracellular 2-NBDG fluorescence (excitation 485 nm, emission 535 nm) was measured (VICTORX4, PerkinElmer, Waltham, MA, USA). Glucose uptake rates were calculated after subtracting the tissue background signal (negative control, without 2-NBDG) and normalized to tissue weights.[21,22]

2.8. Statistical analysis

GraphPad Prism 8 Software was used to perform Student's t test for 2 groups and 1- or 2-way analysis of variance for more groups, followed by Bonferroni's *post hoc* tests. Differences in mean values were considered statistically significant at a probability level of less than 5% ($p < 0.05$). Power of the study was 80–85%, with a confidence level of 95%.

3. Results

3.1. GMC characterization

GMC was produced, purified, bio-compatibilized and characterized by Graphenano Medical Care S.L. from raw CNF (Graphenano S.L., Spain), as detailed in the methods section. Fig. 1A shows the graphene Raman spectrum present in GMC, with a D peak located at 1350 cm^{-1}, which refers to structural defects in the graphene surface, and a G peak at 1570 cm^{-1}, referred to the graphitization grade. GMC intensity D/G peak ratio, which gives the number of structural defects of the material, increased to 1.2, when compared to 0.9 from raw CNF. Fig. 1B shows the GMC crystal structure spectrum, detected by X-ray diffraction, where the diffraction peak of the stacking aromatic structure is $2\theta = 25.9°$, and the peak for the orientation of graphene layer planes is $2\theta = 43.1°$. Interlaminar distance, calculated using Braggs's equation, was 0.344 nm, in accordance with raw CNF values. The average crystalline size in the perpendicular plane of graphene layers is obtained by using Scherrer's equation. Raw CNF presented a crystalline size value of 3.1 nm, whereas GMC was 2.7 nm. Fig. 1C presents the average particle size of GMC in terms of number, with a peak in the order of hundreds of nm and Fig. 1D shows the average particle size in terms of volume, with two peaks at the order of hundreds of nm and thousands of nm. Both spectra were derived from dynamic light scattering, and the Z-average size calculated was around 300 nm. Fig. 1E shows a representative scanning electron microscopy image of GMC, which illustrates a cylindrical structure with a fiber length up to several micrometers and fiber diameters between 5 and 200 nm, like raw CNF.[24] Fig. 1F shows a representative image obtained through high resolution transmission electron microscopy where fibrous particles can be observed with a certain degree of corrugation. These particles are agglomerated among themselves. The range of sizes obtained from the images was between 70 nm to 600 nm, and the average was 300 nm, which corroborates the Z-average size obtained.
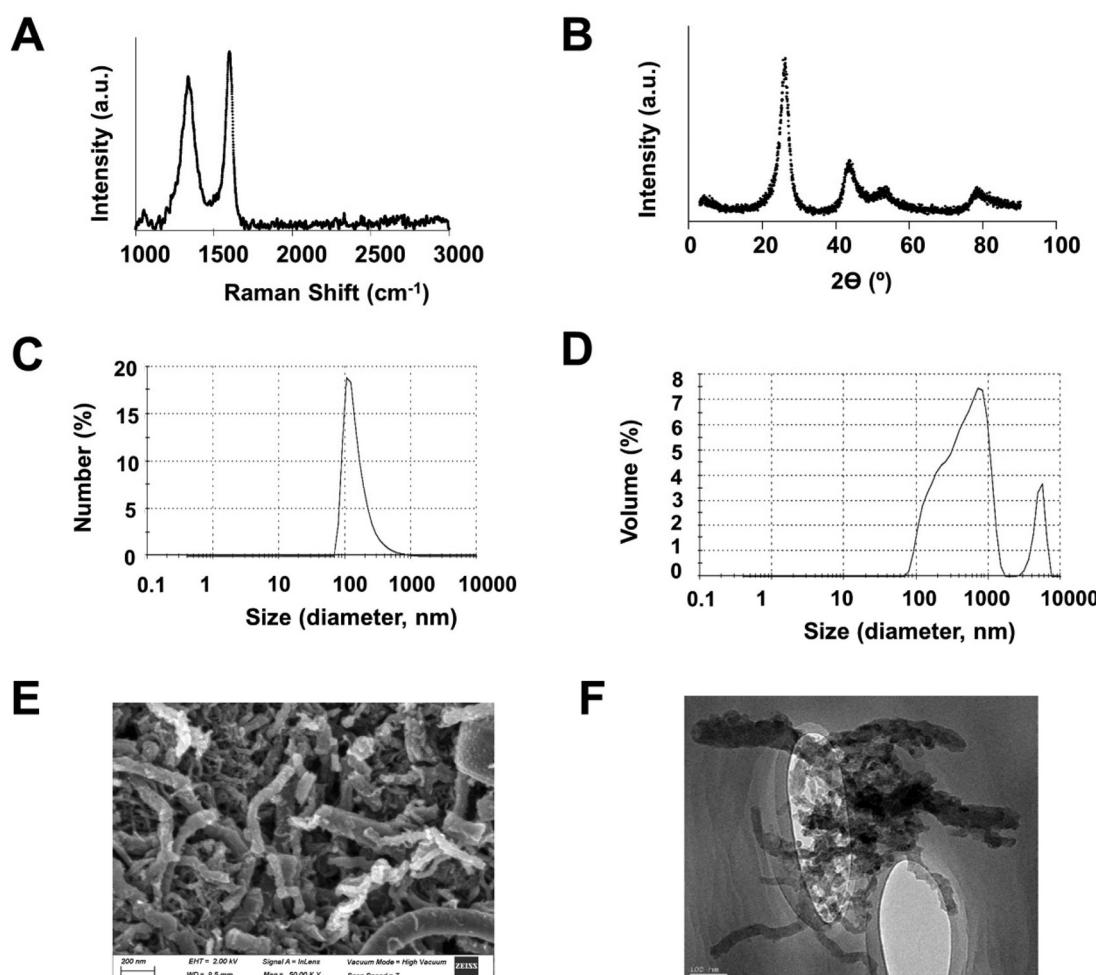
Fig. 1 GMC characterization. Representative data from (A) Raman analysis, (B) X-ray diffraction, (C) number, and (D) volume (in %) of particle size spectra (in nm) derived from dynamic light scattering. (E) Representative image from scanning electron microscopy. (F) Representative image from high resolution transmission electron microscopy.

3.2. GMC used in cultured adipocytes reduces intracellular TG content and adipogenesis markers expression, while increases lipolysis

The *in vitro* functional studies of GMC were performed in cultured fully differentiated adipocytes obtained from adipoblast-like pluripotent cells C3H10T1/2. Fig. 2 shows the quantification of intracellular TG stored in adipocytes LD using lipid-specific dyes. Fig. 2A shows the time-dependent reduction of intracellular TG with 20 μg mL^{-1} of GMC treatment determined by the fluorescent dye AdipoRed, which reaches approximately 40% reduction after 24 h and remains for 72 h. Fig. 2B shows representative microscopical pictures of visually stained LDs from adipocytes using, in this case, colorimetric dye Oil Red O. It can be observed that the change of characteristically large LD in differentiated/hypertrophied adipocytes (CT) to general reduced LD content, which are also smaller and multilocular, in GMC treated cells (20 μg mL^{-1}, 24 h), as corresponding to non-differentiated pre-adipocyte cells.[2,3] Fig. 2C shows GMC dose-dependency of TG reduction at 24 h.

GMC concentrations as low as 5 μg mL^{-1} induced a significant reduction of intracellular TG content (approximately 30%). This reduction was enhanced progressively with higher GMC concentrations. The specificity of GMC in effect was achieved by comparing this functional effect by using other carbon materials in the same time and dose conditions. These molecules were added to the cells for the same time and conditions as GMC: (a) the denaturalized GMC, obtained after the exposition of GMC to 600 °C, which has graphene eliminated from the structure, (b) carbon black, which is a carbon material without CNM properties, (c) GO and (d) rGO, both graphene-based CNM, although carrying different structures compared to GMC. Any of these molecules were able to modify the LD content, thus they were inert/negative in this functional effect observed with GMC (Fig. 2C). The tested GMC concentrations have no relevant effects on the adipocyte cell membranes permeability (trypan blue dye exclusion analysis) or MTT assay (Table 1).

Fig. 3A shows the mRNA expression pattern of several markers after GMC treatment compared with CT in cultured
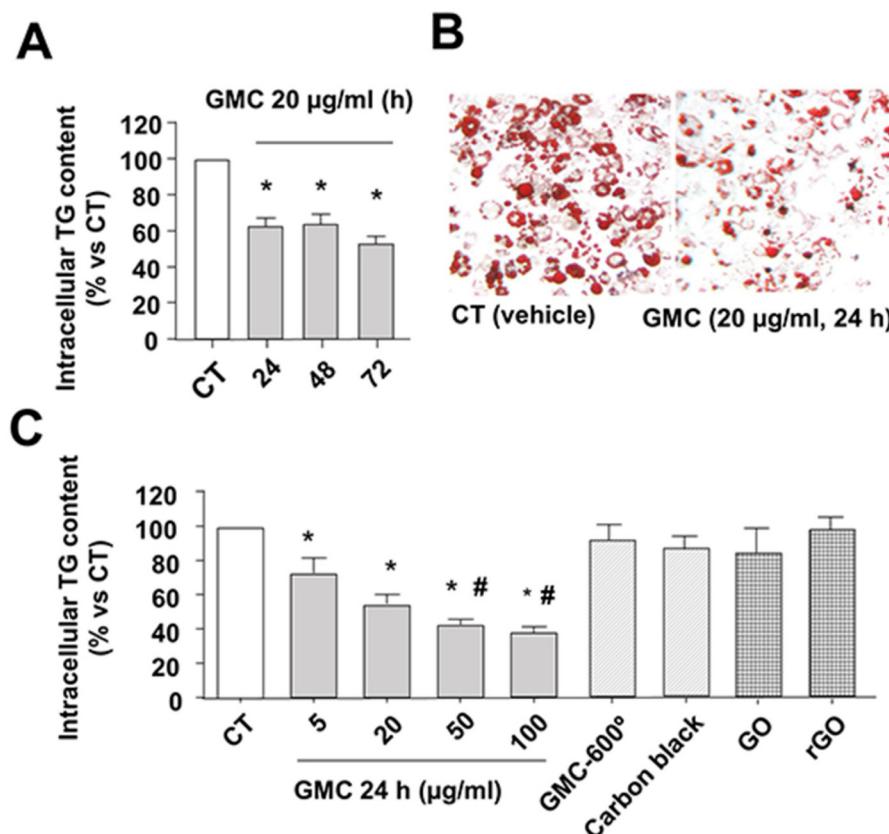
Fig. 2 GMC decreases triglyceride (TG) content in adipocytes. (A) Differentiated adipocytes TG content, quantified with lipid-specific fluorescent dye AdipoRed, after 20 µg mL^{-1} GMC or vehicle (CT) treatments at the indicated times. (B) Representative images of LD stained with Oil-red O inside adipocytes after 24 h treatment (GMC at 20 µg mL^{-1}). (C) Differentiated adipocytes TG content after 24 h of GMC at the indicated concentrations or 20 µg mL^{-1} of three negative controls: denaturalized GMC by exposure to 600 °C (GMC-600°), a non-CNM species (carbon black) and two graphene-based CNM that not share graphene structure with GMC (GO and rGO). Data are expressed as mean $\pm$ standard errors (M $\pm$ SEM) from n = 12 experiments. *$p < 0.05$ vs. CT and #$p < 0.05$ vs. GMC 5 µg mL^{-1}.

Table 1 GMC safety in vitro: adipocytes were treated with GMC at the indicated concentrations or vehicle for 24 h. Viability was determined by trypan blue cellular exclusion, and toxicity was determined by MTT. Data are expressed as mean $\pm$ standard errors (M $\pm$ SEM) from n = 12 experiments

	GMC 5 µg mL^{-1}	GMC 20 µg mL^{-1}	GMC 100 µg mL^{-1}
Adipocytes viability (% vs. vehicle)	101.8 ± 11.2	108.2 ± 11.8	89.1 ± 6.9
Adipocytes MTT (% vs. vehicle)	91.3 ± 1.9	89.4 ± 1.8	90.6 ± 1.6

adipocytes. GMC does not modify the expression of pro-inflammatory cytokines MCP-1 and IL6 while reducing some adipogenesis and mature adipocyte markers such as PPARγ, CEBPB, PGC1-alpha, and adipokine leptin.[2,3,27]

On the other hand, GMC increases the expression of lipolysis markers HSL and lipid metabolite transporters, FABP4, fatty acid translocase FAT, and AQP7.[23,28,29] However, the expression of FASN, the main enzyme for lipogenesis, was also

increased.[30] GMC also increased HSL activity, as shown by the increased protein levels of the active lipolytic isoform (HSL phosphorylated at ser 660) in Fig. 3B.

### 3.3. GMC reduces TG content by a rapid phosphorylation of INT1B and the overexpression of ILK

Fig. 4 shows the involvement of the INTB1/ILK axis during the functional TG decrease caused by GMC in vitro. Fig. 4A shows a rapid and significant phosphorylation in Thr788/9 of INTB1 at 30 min, 1, and 2 h after GMC treatment, which correlates with INTB1 conformational activation.[18] To analyze the relevance of ILK in the genesis of the observed effects, the expression of ILK after GMC treatment was studied in adipocytes. Fig. 4B and C show that GMC increases ILK mRNA and protein levels after 24 h, respectively.

Next, we stated the relevance of INTB1 and ILK in the GMC-induced TG content by (a) blocking INTB1 response and (b) partially depleting ILK before GMC treatment.[23]

We partially depleted ILK transfecting adipocytes with siRNAs against ILK (siILK) or scrambled siRNAS as controls as specified in the methods section. To antagonize INTB1
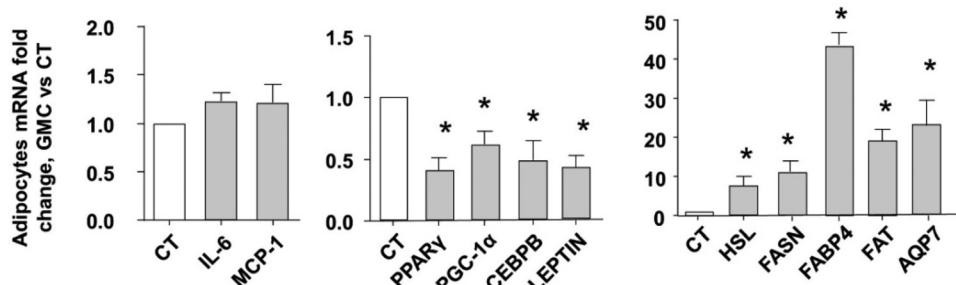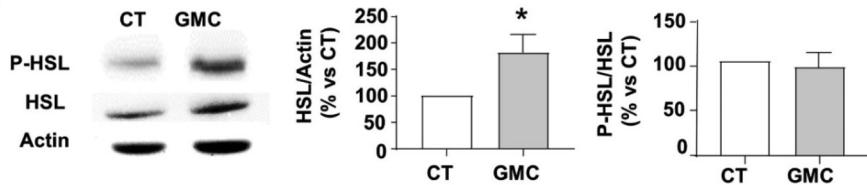
Fig. 3 Inflammation, adipogenesis, and lipolysis markers in adipocytes after GMC treatment. Differentiated adipocytes were treated with 20 μg mL^{-1} GMC or vehicle (CT) for 24 h. (A) mRNA expression fold changes of CT, normalized to β-actin for some inflammation markers (IL-6 and MCP-1), adipogenesis markers (PPARγ, CEBPB, PGC1-alpha, and Leptin), lipolysis and lipogenesis enzymes and lipid transporter proteins (HSL, FASN, FABP4, FAT, and AQP7). (B) HSL total protein content and activity were measured by immunoblot. Representative immunoblots and densitometric analysis of phosphorylated HSL at ser 660 (P-HSL), total HSL and protein contents are given as % of CT. HSL values were normalized to actin as endogenous control, whereas p-HSL values were normalized to total HSL content. Data are expressed as mean ± standard errors (M ± SEM) from n = 12 experiments. *p < 0.05 $vs.$ CT.
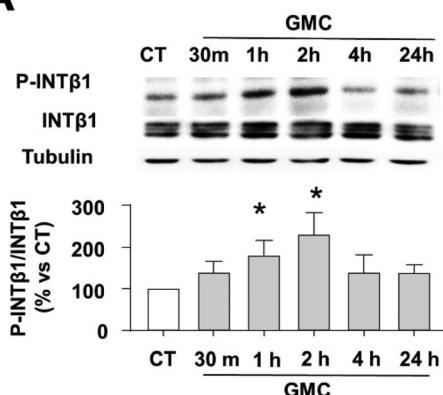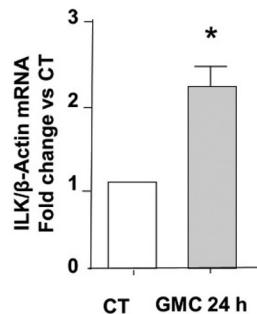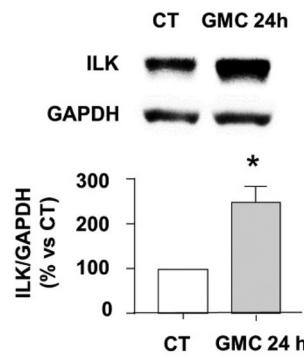

Fig. 4 GMC interacts with integrinβ1 (INTB1) and overexpresses integrin linked kinase (ILK) in adipocytes. Differentiated adipocytes were treated with 20 μg mL^{-1} GMC or vehicle (CT) for the indicated times. (A) Representative immunoblots and densitometric analysis of phosphorylated INTB1 at Thr788/9 (P-INTB1) normalized to total INTB1 (Tubulin blots are shown as charge control). (B) ILK mRNA expression fold changes normalized to β-actin and (C) representative immunoblots and densitometric analysis of total ILK normalized to GAPDH. Data are expressed as mean ± standard errors (M ± SEM) from n = 12 experiments. *p < 0.05 $vs.$ CT.

outside-in signal transduction, we used a very specific function-blocking INTB1 antibody (HMB1, Anti-mouse CD29 clone HMBeta1-1, Biolegend) or irrelevant antibodies (from the same company) in the control cells. In these settings, we added GMC and determined the TG content and ILK expression after 24 h. Fig. 5A shows that HMB1 prevents GMC-dependent TG reduction. Interestingly, ILK depletion (siILK cells) significantly increased TG content compared to CT counterparts, which emphasizes the importance of ILK presence during LD hypertrophy/adipogenesis. On the other hand, GMC was able to partially revert the TG increase of siILK cells, reaching CT values.

Fig. 5B shows that GMC increases ILK mRNA expression, as we already saw in Fig. 4B. This overexpression was dependent
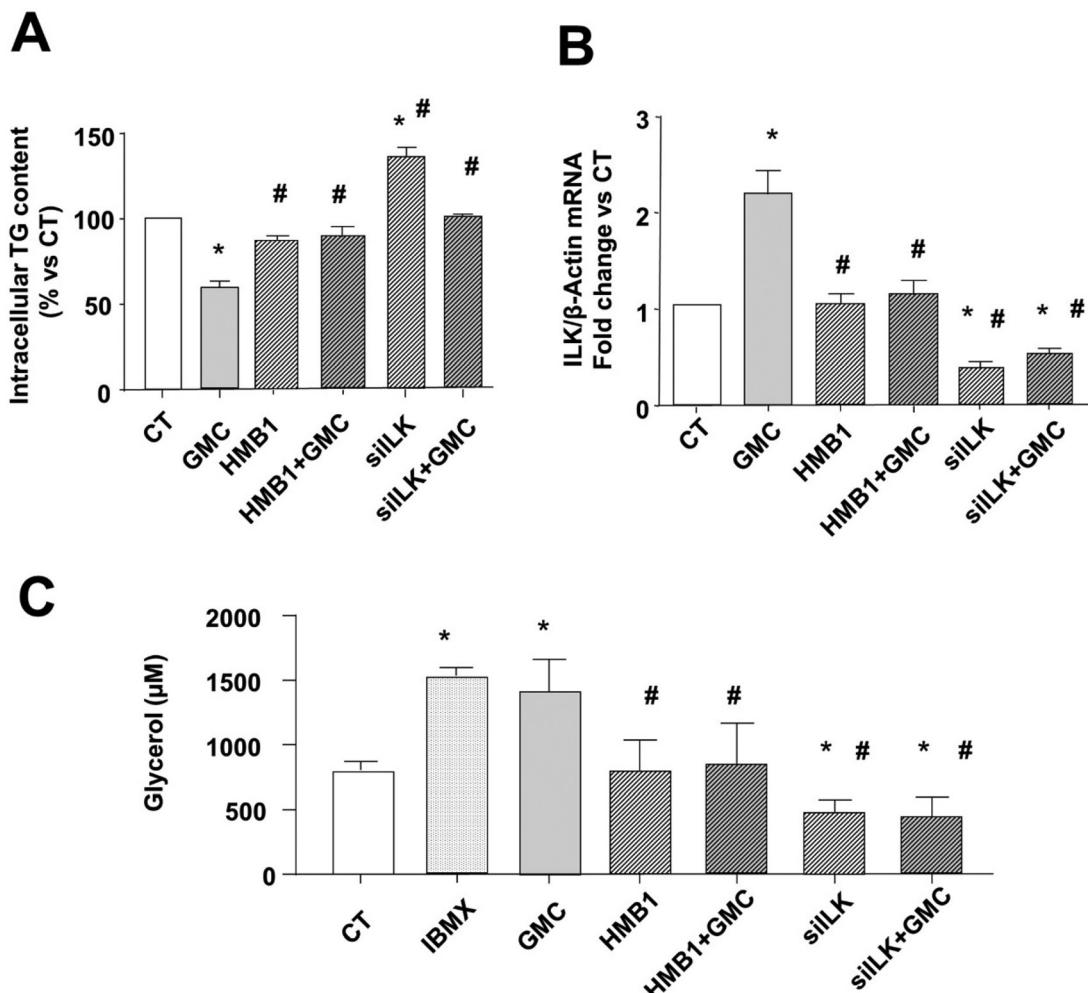
Fig. 5 GMC-dependent lipolytic decrease of triglycerides (TG) in adipocytes is mediated by the interaction with integrinβ1 (INTB1) and integrin linked kinase (ILK). Differentiated adipocytes transfected with either specific siRNAs against ILK (siILK) or scramble siRNAs as controls. 48 h later, transfected adipocytes were treated with either GMC or vehicle (CT) for 24 h. Some of the adipocytes transfected with scramble siRNAs were co-treated with INTB1 blocking antibody (HMB1) or irrelevant antibody together with GMC or vehicle and let for 24 h. (A) Intracellular TG content and (B) ILK mRNA expression fold changes normalized to β-actin. (C) 24 h supernatant glycerol content collected from the treated adipocytes shown in the previous panels. Glycerol from cells treated with 0.5 mM IBMX is shown as a positive control of lipolysis. Data are expressed as mean $\pm$ standard errors (M $\pm$ SEM) from n = 12 experiments. $*p < 0.05$ vs. CT. $\#p < 0.05$ vs. GMC.

on GMC-INTB1 modulation because ILK expression was not upregulated when using HMB1 prior to GMC treatment. In siILK-transfected cells, the successful partial depletion of ILK is visible. Interestingly, GMC-dependent ILK upregulation was invalidated in siILK cells. These results emphasize the relevance of ILK presence during the GMC-dependent intracellular TG balance and the overexpression of ILK itself. Fig. 5C shows that GMC increased glycerol accumulated in the supernatants of the cultured cells, indicating increased intracellular lipolysis, in accordance with the increased expression of lipolysis markers observed in Fig. 3. As a positive control, a single bolus of 0.5 mM IBMX, which activates the PKA-dependent canonical lipolytic pathway, increases the secretion of glycerol in our settings.[23] The blockade of INTB1 or ILK, using HMB1 or siILK, respectively, avoid GMC-mediated lipolysis. Interestingly, siILK

decreases the glycerol content lower than CT, in accordance with the observed TG storage increase in those cells.

3.4. GMC overexpress ILK to promote lipolysis in cultured scWAT explants from mice subjected to High Fat Diet

We previously reported a mice model in which the sixth and seventh exons of ILK gene were excided during young adulthood once they were injected with TX.[21–23] 3 weeks later, the adult mice displaying successful ILK depletion (cKD-ILK) and control littermates (VH-treated, WT) were used. Fig. 6 resumes our approach to study whether GMC or VH modify ILK expression and lipolysis state of hypertrophied scWAT explants,[2,3] obtained from this ILK-depleted mice model once challenged to 6 weeks of high fat diet (HFD) following our previously published protocols[21–23] and detailed in the methods
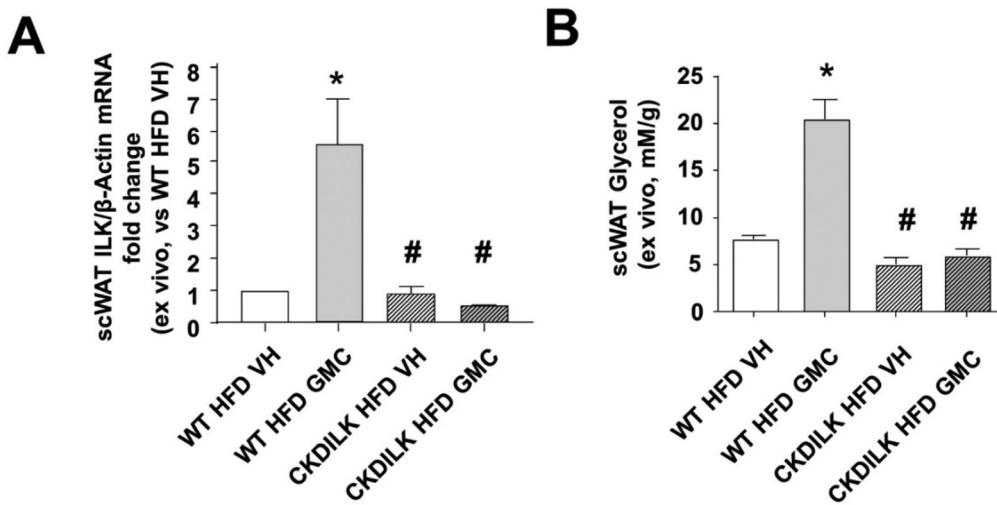
Fig. 6 GMC overexpresses integrin linked kinase (ILK) to promote lipolysis in subcutaneous white adipose tissue (scWAT) from mice challenged with high fat diet (HFD). Conditional Knockdown ILK mice (cKDILK) or wild-type counterparts (WT) were challenged with HFD for a total of 6 weeks. scWAT explants were cultured *ex vivo* in the presence of GMC (20 µg mL^{-1}) or vehicle (CT) for 24 h. (A) ILK mRNA expression fold changes normalized to β-actin. (B) Supernatant glycerol content normalized to grams of scWAT explants. Data are expressed as mean $\pm$ standard errors (M $\pm$ SEM) from $n = 12$ experiments. *$p < 0.05$ *vs.* WT HFD VH. #$p < 0.05$ *vs.* WT HFD GMC.

section. Explants of scWAT from these animals were treated *in vitro* in the same conditions as the adipocytes, with either VH or GMC for 24 h. Fig. 6A shows that GMC treatment increases ILK expression in scWAT explants from HFD-control animals (WT), an effect that was not observed when GMC was administered to HFD-mice with ILK depleted in scWAT. The levels of lipolysis metabolite glycerol were also increased in the supernatants after GMC treatment on HFD-WT scWAT explants, while the depletion of ILK in HFD-cKDILK scWAT prevented this effect (Fig. 6B).

3.5. GMC topical application in rats subjected to HFD reduces body and scWAT weights while overexpress ILK

To elucidate whether GMC may decrease scWAT hypertrophy *in vivo*, rats were challenged with STD or HFD for 5 weeks to settle a diet-induced increase of scWAT size,[25] and therefore GMC (100 µg mL^{-1}) or vehicle (VH, paraffin) were topically applied on the depilated dorsal-inguinal areas of the animals.[26] The application was performed with massage 2 times per day for a total period of 5 days while the animals were maintained in their respective diets. No difference in daily food or water intake was observed between the different experimental groups (data not shown). Fig. 7A shows total body weight (BW) gain, along the week of the topical applications. In VH-treated HFD-fed rats, BW was increased by more than 25% when compared to control STD-fed rats. GMC application reduced BW gains in either STD or HFD groups when compared to their respective control rats (VH-treated). Fig. 7B shows that the weights of the dorsal-inguinal scWAT pads extracted after the experimentation were in accordance with BW changes. Fig. 7C shows that topical GMC application overexpressed ILK in scWAT from HFD-fed rats, in accordance with the results observed *in vitro* and *ex vivo*. Some markers for

renal, hepatic, and inflammatory safeness were determined in the blood of HFD-fed rats treated topically with GMC.

No differences between experimental groups were observed for plasma creatinine, aspartate amino transferase, as well as IL-1β mRNA expression in peripheral blood mononuclear cells (Table 2).

Because we previously published that reduced ILK levels are related with early glycaemic imbalance, and taking into consideration that GMC changes ILK-related mechanisms, we wonder whether GMC also affects glycaemia and/or the main glucose transporter in WAT, GLUT4.[21–23] GMC treatments did not change GLUT4 expression compared to controls, neither in cultured adipocytes nor in cultured scWAT explants from STD-fed WT. The extracellular glucose uptake capacity was not different in WT WAT explants treated with GMC, compared to vehicle-treated controls after the stimulation with insulin, which canonically increased the traffic of GLUT4 and its presence in the membrane (the glucose uptake was detected intracellularly with the use of a fluorescent glucose analogue, 2-NBDG, as specified in methods). Finally, glycaemia levels were not different in STD-fed rats where GMC was topically applied, compared to VH-treated (ESI†).

4. Discussion

This is the first study to describe that a graphene-based material reduces triglyceride inside adipocytes and therefore, WAT hypertrophy in the DIO model. We demonstrated that GMC, a CNF-based material with graphene in its structure and an average particle size of hundreds of nm, can be safely used in concentrations lower than 150 µg mL^{-1}, because it has non-toxic effects on cultured adipocytes, in accordance with the
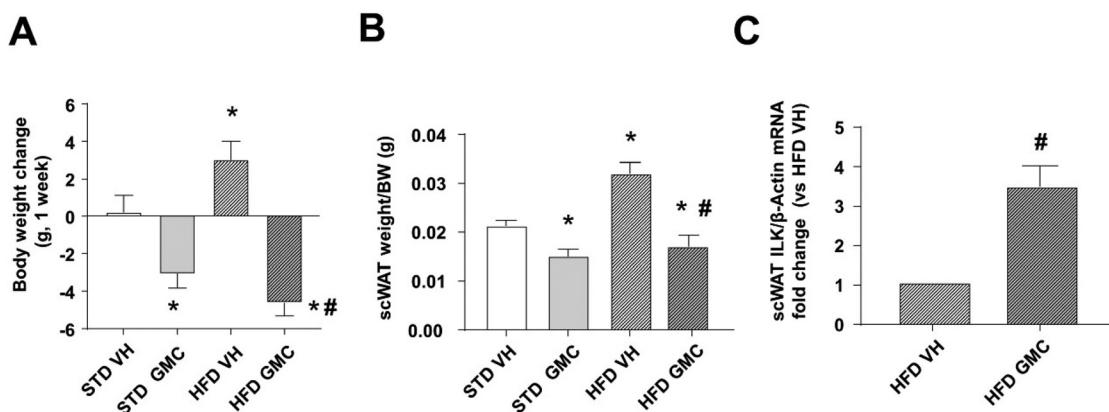
Fig. 7 Topical administration of GMC in rats challenged with high fat diet (HFD) reduces total body and subcutaneous white adipose tissue (scWAT) weights and overexpress integrin linked kinase (ILK). Rats were challenged to HFD or standard diet (STD) for a total of 6 weeks. Along the 5th week, animals were depilated in the dorsal-inguinal area and subjected to topical applications of 100 μg mL^{-1} GMC or vehicle (VH) 2 times per day for 5 consecutive days. (A) Total gain of body weight (BW), (B) scWAT weights normalized to BW after the treatment and (C) ILK mRNA expression fold changes in scWAT from HFD-treated rats, normalized to β-actin. Data are expressed as mean ± standard errors (M ± SEM) from $n = 12$ experiments. *$p < 0.05$ vs. STD VH. #$p < 0.05$ vs. HFD GMC.

Table 2 GMC safety *in vivo*: HFD rats were depilated in the dorsal-inguinal area and subjected to topical applications of 100 μg mL^{-1} GMC or vehicle enhanced with massage 2 times per day for 5 consecutive days. At the end of the treatments, plasmatic creatinine and aspartate aminotransferase and peripheral blood mononuclear cells (PBMC) IL-1β mRNA levels were determined and normalized to β-actin. Data are expressed as mean ± standard errors (M ± SEM) from $n = 12$ experiments

	Vehicle	GMC
Creatinine (plasma, μg dl^{-1})	380 ± 30	370 ± 40
Aspartate Aminotransferase (plasma, U l^{-1})	200 ± 25	210 ± 23
IL-1beta levels in PBMC (mRNA fold changes *vs.* vehicle)	1.1 ± 0.5	1.2 ± 0.4

safe concentration stated in previous work on skin cells,[10] while has a functional effect promoting adipocyte trans-differentiation to a catabolic phenotype. Each CNM member, as in the case of GMC, exhibits different carbon arrangements, size, and physicochemical properties, which lend unique and characteristic interactions with biomolecules, cells, and tissues, and therefore may induce effects that vary from inert to bioactive or toxic.[6,7] In this context, the ability for different CNM to module stem cell differentiation during osteogenesis, chondrogenesis, or neurogenesis has been analyzed,[11,31–33] including CNF.[9] In some of those publications, GO, and CNT have been reported to indirectly modulate adipogenesis, but the present study is the first to deeply analyze the CNF-based capacity in modifying adipogenesis during obesity.

We demonstrate that the functional capacity to reduce TG content in adipocytes was very specific to GMC and the particular disposition of graphene on it because the effect was not replicated by other carbon materials or CNM that have or did not have graphene in their structures, such as carbon black, GO, rGO or GMC with a denaturalized structure (GMC exposed to 600 °C).

Once GMC interacts with the adipocytes, the intracellular changes may be summarized as follows: (a) TG content inside LD decreases, the expression and activity of main lipase HSL as well as the excretion of the lipolysis marker glycerol and the expression of lipolysis metabolites transporters (FABP4, FAT, and AQP7)[28,29] were all increased, while (b) adipogenesis-related transcription factors (PPARγ, CEBP, and PGC1-alpha)[27] and leptin, the main adipokine that represents adipose hypertrophy[3] decreased. Finally, (c) GMC did not evoke inflammation because the expression of adipocytokines IL-6 and MCP1 were not affected, as well as the glucose transporter GLUT4.

Although we demonstrated that GMC increases lipolysis (reduced TG content because of increased HSL activity and excreted glycerol), the expression of the main enzyme for lipogenesis, FASN, was increased in the trans-differentiating adipocytes. This may remain as a paradoxical effect. Lipolysis and lipogenesis are two events intimately related but not necessarily conflicting: impaired FASN has been linked to metabolic disorders.[30] Related to this observation, a high transcriptional upregulation of FASN may be linked to insulin-sensitivity improvement.[34] Therefore, we hypothesize that GMC-dependent FASN upregulation is part of feedback during adipocyte de-differentiation. However, the goal of the present work is to demonstrate the capacity of GMC to reduce fat deposition and indeed, the net effect was the reduction of intracellular TG content despite FASN content.

The physicochemical mechanisms modulating cellular adhesion, spreading, and differentiation by other graphene-based CNM are not well defined but allowed us to intuit that the graphene present in GMC could act as an artificial biophysical cue like the natural ECM components, which interacts with INT and its intracellular downstream interactome.[11–16] ILK is a major INTB1 scaffold protein of the interactome recruited to modulate the cytoskeleton.[19] We demonstrated in

cultured adipocytes that GMC rapidly phosphorylated INTB1 at Thr788/9 and activated outside-in signaling, which is intimately related with adipogenesis.[17,18] The blockade of INTB1 with HMB1 antibody avoids the GMC effect on triglyceride content and lipolysis. Importantly, GMC also increased ILK content, and this was blocked by HMB1. All the changes mediated by GMC were dependent on ILK presence because the ILK blockade using siILK induces similar changes to those elicited by HMB1. Conclusively, we suggest that GMC interacts with INTB1/ILK axis on adipocytes to lead to trans-differentiating mechanisms that decrease lipid content. We further performed studies in scWAT explants ex vivo and in vivo from obese rodents. scWAT depots are responsible for storing over 80% of total body fat, and their principal adaptation to obesity relates to hypertrophy of the tissue.[2,3] GMC treatment in hypertrophied scWAT explants confirms the dependency of INTB1/ILK described in the cultured adipocytes model because GMC-induced lipolysis and ILK overexpression were avoided on explants where INTB1 or ILK was blocked. As a pre-clinical approach, the topical application of GMC in overweighted rats induced the reduction of scWAT weights with the subsequent decrease in total body weight.

Here, we demonstrated that GMC, via INTB1 and ILK, is probably modulating the transcription of several adipose-related genes, as well as ILK itself. The transcriptional regulation mediated by graphene is understudied: so far, some publications stated that CNM-based structures may interact with INT to modify the expression of several genes, but taking into consideration the different physiological contexts under study,[12–15] and some of these publications linked ILK during the process.[14,16] As expected, the ILK transcriptional activity on other genes may use multiple substrates, according to the vast range of functions where it has been implicated;[19] for example, we previously published that ILK was able to regulate transcriptional factors NFATc and AP1 during the expression of water channel Aquaporin 2.[35] In accordance, our results point to a transcriptional mechanism inside the adipocyte driven by GMC-INT-ILK, and within GMC-INT activation and ILK-mediated transcription, a potential mediator may be Rho-associated protein kinase (ROCK), because it has been linked during GO interaction with INT[36] and recurrently pointed to be a mediator after ILK activation.[37,38] About the transcription of the ILK gene, several transcriptional factors can be responsible for the modulation, such as AP-2, Sp1, NF-κβ, EGR1, Ets-1, or HIF-α, due to the motifs variety present in ILK promoter.[19] However, further studies should be devoted to understanding the transcriptional regulation followed by the activation of the axis GMC/INTB1/ILK.

In any case, a very relevant statement from the present work is the importance of ILK expression levels during adipocyte differentiation; GMC increased ILK yield and reduced adipocytes hypertrophy in all the experimental approaches, in vitro, ex vivo, and in vivo, and these results are in accordance with our previously stated hypothesis: (a) ILK expression is decreased during the development of obesity, (b) WAT transgenic downregulation of ILK (in cKD-ILK) exacerbates the

obesity-related symptoms and finally, (c) overexpression of WAT ILK can ameliorate obesity.[21–23] The opposite hypothesis has been stated in Bugler-Lamb's work,[20] where ILK expression was increased by a long-term HFD and the use of adipocyte-specific ILK-deficient mice and ILK knockdown in 3T3-L1 displayed reduced fat mass. Differences in methodological and conceptual approaches between Bugler-Lamb's models and ours may explain the apparently contradictory results between studies. Nevertheless, here, we did carry out a pharmacological strategy to increase ILK expression in vitro and in vivo as a protective approach against obesity that was not used in Bugler-Lamb's study. Because GMC biocompatibility in vivo was still unknown, we chose to apply it topically, a less invasive administration pathway compared with others that may be potentially more aggressive:[25] according to previous works, systemic administration (e.g., Intraperitoneal) of CNM similar to GMC is shown to be incompatible.[39,40] The topical administration of GMC in vivo was apparently biocompatible (no changes in systemic toxicity parameters, as shown in Table 2), and it has an effect on the underlying scWAT, posing an interesting question concerning GMC transdermal absorption. On intact skin, topically applied drugs may use different transdermal pathways (intercellular, intracellular, or through hair follicles and other skin glands) to penetrate, and the penetration ability depends on several factors such as particle size, lipid composition in the application area or the use of external forces or enhancers, which facilitate the process (e.g., massage, microneedles, electroporation).[26,41,42] According to different studies, the cut-off size of the molecules to percutaneously be absorbed may vary from dozens to hundreds or even thousands of nanometers when the application is helped by mechanical forces.[43,44] In our studies, it is reasonable to consider the penetration of GMC through the skin to modify the size and genetic expression pattern of the scWAT layer under the region where it was applied, probably due to the conjunction of size and the motion caused by the massage during its application. Unfortunately, we were unable to observe GMC reaching the hypodermis because it is difficult to trace carbon-based structures of CNM in tissues in such a small amount; moreover, if it is not tagged, neither has intrinsic fluorescence.[45] It is possible that other WAT depots (e.g., epiWAT) may be implicated in the total body weight loss observed after the topical application and GMC may be systemically absorbed and targeting adipocytes of distant depots from the located application. It is, therefore, reasonable that whether GMC has been systemically absorbed, it may reach other organs. To study whether topically applied GMC has other functional effects in other organs was out of the present work. As explained before, to study the pharmacokinetics of a non-tagged carbon-based structure may be extremely difficult. Nevertheless, we demonstrate that the topical application for several days in vivo was safe because it did not alter inflammation or other systemic damage markers. In conclusion, GMC binds to adipocytes INTB1/ILK cluster to trans-differentiate them to reduce intracellular lipid accumulation, adipogenesis, and cellular hypertrophy while increasing lipolysis without inflammation.

Overexpression of ILK takes place, perpetuating GMC positive effects. Pre-clinical studies have shown that GMC topical administration reduces scWAT weight gain in DIO rodents.

5.   Conclusions

We demonstrate for the first time that a CNF-based product with graphene content in its structure is safe and effective in reducing scWAT size when topically applied *in vivo*. GMC binds to adipocytes INTB1 to reduce TG content and transcriptionally downregulate adipogenesis and upregulate lipolysis. ILK presence is necessary for this mechanism. GMC in turn increases ILK expression, which demonstrates that Graphene presence and ILK upregulation may be considered for anti-obesogenic strategies.

Abbreviations

AQP7	Aquaglyceroporin 7
BW	Body weight
CEBP	CCAAT/enhancer-binding protein beta
cKDILK	ILK knock-down mice
CNF	Carbon nanofibers
CNM	Carbon nanomaterial
CNT	Carbon nanotubes
CT	Control, vehicle-treated cells
ECM	Extracellular matrix
FABP4	Fatty Acid Binding Protein 4
FASN	Fatty acid synthase
FAT	Fatty Acid Translocase
GAPDH	Glyceraldehyde 3-phosphate dehydrogenase
GLUT4	Glucose transporter type 4
GMC	The new graphene-based carbon nanomaterial
GO	Graphene oxide
HFD	High fat diet
HMB1	Anti-mouse CD29 clone HMBeta1-1, INTB1 blocking antibody
HSL	Hormone Sensitive Lipase
IBMX	3-Isobutyl-1-methylxanthine
IL-1β	Interleukin-1β
IL-6	Interleukin-6
ILK	Integrin-linked kinase
INT	Integrin
INTB1	Integrin-β1
LD	Lipid droplets
MCP-1	Monocyte chemoattractant protein-1
MTT	Mitochondrial metabolic activity
PBMC	Peripheral blood mononuclear cells
PGC1-alpha	Peroxisome Proliferator-activated Receptor Gamma-coactivator-Alpha
P-HSL	HSL active isoform, phosphorylated at ser660
P-INTB1	INTB1 active isoform, phosphorylated at thr 788/9
PPARγ	Peroxisome proliferator activated receptor gamma
rGO	Reduced Graphene oxide
RT-qPCR	Reverse transcription–quantitative polymerase chain reaction
scWAT	Subcutaneous WAT depot
siILK	Silencing RNA against ILK
siRNA	Silencing RNA
STD	Standard diet
TG	Triglycerides
VH	Vehicle
WAT	White adipose tissue
WT	Wildtype mice

Author contributions

MRP and DRP directed the work equally. SDF, MRP, DRP conceived the study. SDF designed the experimental plan, performed experiments, and wrote the manuscript. MG and PLL performed experiments, analyzed, and interpreted the data. PLL, MMR and JAMR critically revised the intellectual content of the project. All authors approved the final submitted version.

Conflicts of interest

Acknowledgements

References

1 U. White and E. Ravussin, *Diabetologia*, 2019, **62**(1), 17–23, DOI: **10.1007/s00125-018-4732-x**.

2 Q. A. Wang, C. Tao, R. K. Gupta and P. E. Scherer, *Nat. Med.*, 2013, **19**(10), 1338–1344, DOI: **10.1038/nm.3324**.

3 A. Booth, A. Magnuson, J. Fouts and M. T. Foster, *Horm. Mol. Biol. Clin. Invest.*, 2016, **26**(1), 25–42, DOI: **10.1515/hmbci-2015-0073**.

4 B. D. Pope, C. R. Warren, K. K. Parker and C. A. Cowan, *Trends Cell Biol.*, 2016, **26**(10), 745–755, DOI: **10.1016/j.tcb.2016.05.005**.

5 W. C. Lee, C. H. Lim, H. Shi, L. A. Tang, Y. Wang, C. T. Lim and K. P. Loh, *ACS Nano*, 2011, **5**(9), 7334–7341, DOI: 10.1021/nn202190c.

6 T. M. Magne, T. de Oliveira Vieira, L. M. R. Alencar, F. F. M. Junior, S. Gemini-Piperni, S. V. Carneiro, L. M. U. D. Fechine, R. M. Freire, K. Golokhvast, P. Metrangolo, P. B. A. Fechine and R. Santos-Oliveira, *J. Nanostruct. Chem.*, 2021, **6**, 1–35, DOI: 10.1007/s40097-021-00444-3.

7 V. Georgakilas, J. A. Perman, J. Tucek and R. Zboril, *Chem. Rev.*, 2015, **115**(11), 4744–4822, DOI: 10.1021/cr500304f.

8 N. Saito, K. Aoki, Y. Usui, M. Shimizu, K. Hara, N. Narita, N. Ogihara, K. Nakamura, N. Ishigaki, H. Kato, H. Haniu, S. Taruta, Y. A. Kim and M. Endo, *Chem. Soc. Rev.*, 2011, **40**(7), 3824–3834, DOI: 10.1039/c0cs00120a.

9 P. A. Tran, L. Zhang and T. J. Webster, *Adv. Drug Delivery Rev.*, 2009, **61**(12), 1097–1114, DOI: 10.1016/j.addr.2009.07.010.

10 B. Salesa, M. Assis, J. Andrés and Á. Serrano-Aroca, *Biomedicines*, 2021, **9**(9), 1155, DOI: 10.3390/biomedicines9091155.

11 M. Rahmati and M. Mozafari, *Front. Bioeng. Biotechnol.*, 2019, **7**, 4, DOI: 10.3389/fbioe.2019.00004.

12 H. Xie, T. Cao, A. Franco-Obregón and V. Rosa, *Int. J. Mol. Sci.*, 2019, **20**(3), 574, DOI: 10.3390/ijms20030574.

13 R. Ikram, S. A. A. Shamsuddin, B. Mohamed Jan, M. Abdul Qadir, G. Kenanakis, M. M. Stylianakis and S. H. Anastasiadis, *Molecules*, 2022, **27**(2), 379, DOI: 10.3390/molecules27020379.

14 S. Shah, P. T. Yin, T. M. Uehara, S. T. Chueng, L. Yang and K. B. Lee, *Adv. Mater.*, 2014, **26**(22), 3673–3680, DOI: 10.1002/adma.201400523.

15 S. D. Newby, T. Masi, C. D. Griffin, W. J. King, A. Chipman, S. Stephenson, D. E. Anderson, A. S. Biris, S. E. Bourdo and M. Dhar, *Int. J. Nanomed.*, 2020, **15**, 2501–2513, DOI: 10.2147/IJN.S245801.

16 G. Yue, W. Song, S. Xu, Y. Sun and Z. Wang, *Biomater. Sci.*, 2019, **7**(3), 975–984, DOI: 10.1039/c8bm01151f.

17 F. J. Ruiz-Ojeda, J. Wang, T. Bäcker, M. Krueger, S. Zamani, S. Rosowski, T. Gruber, Y. Onogi, A. Feuchtinger, T. J. Schulz, R. Fässler, T. D. Müller, C. García-Cáceres, M. Meier, M. Blüher and S. Ussar, *Mol. Metab.*, 2021, **45**, 101147, DOI: 10.1016/j.molmet.2020.101147.

18 S. Nilsson, D. Kaniowska, C. Brakebusch, R. Fässler and S. Johansson, *Exp. Cell Res.*, 2006, **312**(6), 844–853, DOI: 10.1016/j.yexcr.2005.12.001.

19 A. Górska and A. J. Mazur, *Cell. Mol. Life Sci.*, 2022, **79**(2), 100, DOI: 10.1007/s00018-021-04104-1.

20 A. R. Bugler-Lamb, A. Hasib, X. Weng, C. K. Hennayake, C. Lin, R. J. McCrimmon, R. H. Stimson, M. L. J. Ashford, D. H. Wasserman and L. Kang, *Mol. Metab.*, 2021, **49**, 101197, DOI: 10.1016/j.molmet.2021.101197.

21 M. Hatem-Vaquero, M. Griera, D. Garcia-Ayuso, S. Campillo, L. Bohorquez, L. Calleros, D. Rodriguez-Puyol, M. Rodriguez-Puyol and S. de Frutos, *Cell. Physiol. Biochem.*, 2020, **54**(1), 71–87, DOI: 10.33594/000000206.

22 M. Hatem-Vaquero, M. Griera, A. García-Jerez, A. Luengo, J. Álvarez, J. A. Rubio, L. Calleros, D. Rodríguez-Puyol, M. Rodríguez-Puyol and S. De Frutos, *J. Endocrinol.*, 2017, **234**(2), 115–128, DOI: 10.1530/JOE-16-0662.

23 S. de Frutos, M. Griera, M. Hatem-Vaquero, S. Campillo, E. Gutiérrez-Calabres, D. García-Ayuso, M. Pardo, L. Calleros, M. Rodríguez-Puyol and D. Rodríguez-Puyol, *Cell Biosci.*, 2022, **12**(1), 10, DOI: 10.1186/s13578-022-00746-1.

24 G. Zou, D. Zhang, C. Dong, H. Li, K. Xiong, L. Fei and Y. Qian, *Carbon*, 2006, **44**, 828–832, DOI: 10.1016/j.carbon.2005.10.035.

25 K. S. Gollisch, J. Brandauer, N. Jessen, T. Toyoda, A. Nayer, M. F. Hirshman and L. J. Goodyear, *Am. J. Physiol. Endocrinol. Metab.*, 2009, **297**(2), E495–E504, DOI: 10.1152/ajpendo.90424.2008.

26 Z. Li, X. Fang and D. Yu, *Int. J. Mol. Sci.*, 2021, **22**(23), 12754, DOI: 10.3390/ijms222312754.

27 U. A. White and J. M. Stephens, *Mol. Cell. Endocrinol.*, 2010, **318**(1–2), 10–14, DOI: 10.1016/j.mce.2009.08.023.

28 J. Storch and A. E. Thumser, *Biochim. Biophys. Acta*, 2000, **1486**, 28–44, DOI: 10.1016/S1388-1981(00)00046-9.

29 A. Rodríguez, V. Catalán, J. Gómez-Ambrosi and G. Frühbeck, *Cell Cycle*, 2011, **10**(10), 1548–1556, DOI: 10.4161/cc.10.10.15672.

30 I. Moreno-Indias and F. J. Tinahones, *J. Diabetes Res.*, 2015, **2015**, 970375, DOI: 10.1155/2015/970375.

31 S. R. Ryoo, Y. K. Kim, M. H. Kim and D. H. Min, *ACS Nano*, 2010, **4**(11), 6587–6598, DOI: 10.1021/nn1018279.

32 M. Patel, H. J. Moon, Y. Ko du and B. Jeong, *ACS Appl. Mater. Interfaces*, 2016, **8**(8), 5160–5169, DOI: 10.1021/acsami.5b12324.

33 J. Kim, K. S. Choi, Y. Kim, K. T. Lim, H. Seonwoo, Y. Park, D. H. Kim, P. H. Choung, C. S. Cho, S. Y. Kim, Y. H. Choung and J. H. Chung, *J. Biomed. Mater. Res., Part A*, 2013, **101**(12), 3520–3530, DOI: 10.1002/jbm.a.34659.

34 Y. Wang, B. Jones Voy, S. Urs, S. Kim, M. Soltani-Bejnood, N. Quigley, Y. R. Heo, M. Standridge, B. Andersen, M. Dhar, R. Joshi, P. Wortman, J. W. Taylor, J. Chun, M. Leuze, K. Claycombe, A. M. Saxton and N. Moustaid-Moussa, *J. Nutr.*, 2004, **134**(5), 1032–1038, DOI: 10.1093/jn/134.5.1032.

35 M. Hatem-Vaquero, M. Griera, W. Giermakowska, A. Luengo, L. Calleros, L. V. Gonzalez Bosc, D. Rodríguez-Puyol, M. Rodríguez-Puyol and S. De Frutos, *Biochim. Biophys. Acta, Gene Regul. Mech.*, 2017, **1860**(9), 922–935, DOI: 10.1016/j.bbagrm.2017.07.006.

36 J. Zhu, M. Xu, M. Gao, Z. Zhang, Y. Xu, T. Xia and S. Liu, *ACS Nano*, 2017, **11**(3), 2637–2651, DOI: 10.1021/acsnano.6b07311.

37 A. Graness, K. Giehl and M. Goppelt-Struebe, *Cell. Signalling*, 2006, **18**(4), 433–440, DOI: 10.1016/j.cellsig.2005.05.011.

38 Y. Izawa, Y. H. Gu, T. Osada, M. Kanazawa, B. T. Hawkins, J. A. Koziol, T. Papayannopoulou, M. Spatz and G. J. Del

Zoppo, *J. Cereb. Blood Flow Metab.*, 2018, **38**(4), 641–658, DOI: **10.1177/0271678X17722108**.

39 X. Liu, Q. Guo, Y. Zhang, J. Li, R. Li, Y. Wu, P. Ma and X. Yang, *Dose-Response*, 2016, **14**(4), 1559325816681320, DOI: **10.1177/1559325816681320**.

40 F. Xiaoli, C. Qiyue, G. Weihong, Z. Yaqing, H. Chen, W. Junrong and S. Longquan, *Arch. Toxicol.*, 2020, **94**(6), 1915–1939, DOI: **10.1007/s00204-020-02717-2**.

41 S. H. Park, M. R. Hyun and S. W. Kim, *Aesthetic Plast. Surg.*, 2019, **43**(6), 1657–1662, DOI: **10.1007/s00266-019-01514-2**.

42 T. W. Prow, J. E. Grice, L. L. Lin, R. Faye, M. Butler, W. Becker, E. M. Wurm, C. Yoong, T. A. Robertson, H. P. Soyer and M. S. Roberts, *Adv. Drug Delivery Rev.*, 2011, **63**(6), 470–491, DOI: **10.1016/j.addr.2011.01.012**.

43 A. Vogt, B. Combadiere, S. Hadam, K. M. Stieler, J. Lademann, H. Schaefer, B. Autran, W. Sterry and U. Blume-Peytavi, *J. Invest. Dermatol.*, 2006, **126**(6), 1316–1322, DOI: **10.1038/sj.jid.5700226**.

44 J. Lademann, H. Richter, S. Schanzer, F. Knorr, M. Meinke, W. Sterry and A. Patzelt, *Eur. J. Pharm. Biopharm.*, 2011, **77**(3), 465–468, DOI: **10.1016/j.ejpb.2010.10.015**.

45 C. Deeney, E. P. McKiernan, S. A. Belhout, B. J. Rodriguez, G. Redmond and S. J. Quinn, *Molecules*, 2019, **24**(8), 1455, DOI: **10.3390/molecules24081455**.